Facile and scalable synthesis of Cu2O-SnO2 catalyst for the photoelectrochemical CO2 conversion

Catalysis Today 413-415 (2023) 113985

Contents lists available at ScienceDirect

Catalysis Today

journal homepage: www.elsevier.com/locate/cattod

Facile and scalable synthesis of Cu_2O-SnO_2 catalyst for the photoelectrochemical CO_2 conversion

Maddalena Zoli [a], Daniela Roldán [a], Hilmar Guzmán [a], Micaela Castellino [a], Angelica Chiodoni [b], Katarzyna Bejtka [c], Nunzio Russo [a], Simelys Hernández [a,*]

[a] CREST group, Department of Applied Science and Technology (DISAT), Politecnico di Torino, Turin, Italy
[b] Center for Sustainable Future Technologies, IIT@Polito, Istituto Italiano di Tecnologia, Turin, Italy
[c] Department of Applied Science and Technology (DISAT), Politecnico di Torino, Turin, Italy

ARTICLE INFO

Keywords:
Cu_2O-SnO_2
Photocathodes
Photoelectrode
CO_2 reduction
Cu restructuration
Cu_2O stabilization
Cu^{+1}
Photocorrosion

ABSTRACT

CO2 conversion into high-value-added products is becoming increasingly attractive to find substitutes for fossil-based ones and tackle the environmental crisis. Herein, a noble, simple, reproducible, and scalable Cu_2O-SnO_2 photo-electrocatalyst was synthesized and characterized. Coupling cuprous oxide with tin oxide allowed for protecting unstable Cu^{+1} species from photo-corrosion. Evidence of the SnO_2 stabilization role were found via chronoamperometry tests under chopped light and XPS analysis. An optimized catalytic ink was developed to prepare the photocathodes. The CO_2 photo-electroreduction tests demonstrated a prevalent production of CO and formate with Faradaic efficiencies of 35.47 % and 19.58 %, respectively, and a good system stability. Sunlight illumination demonstrated to play a major role to hinder H_2 evolution and promote $\geq C_{1+}$ products formation.

1. Introduction

The CO_2 is a fully oxidised, inert and stable molecule; thus, its conversion to other C-based molecules is difficult without a substantial energy input [1], but the rewards are potentially huge. In this work, we focused on the CO_2 reduction reaction (CO_2RR) path directed towards products like CO and formate, for which the transfer of $2e^-$ is required. Recently, large interest has been devoted to the copper oxide-based materials for their various applications and their ability to reduce CO_2 to valuable products with a relevant activity [1,2]. Cuprous oxide (Cu_2O) is a p-type semiconductor with an excellent visible light absorption ability, as shown by its band gap of ~ 2 eV, and a favourable conduction band position [3,4]. The suitable positioning of its conduction and valence bands makes Cu_2O an ideal photocatalyst for CO_2RR to CO and C_1 compounds like formic acid, because its Fermi level has lower energy than the standard reduction potential of the CO_2/CO couple ($E^\circ = -0.105$ V vs. NHE at pH=0) and CO_2/HCOOH couple ($E^\circ = -0.169$ V vs. NHE at pH=0) [5]. Nevertheless, as commonly described for photoactive semiconductors, its photo-stability is insufficient for their application in large-scale devices or facilities [6]. The main limitation is that the catalyst initial photoactivity decreases in short time. An efficient charge transfer can prevent the possibility of self-photo-reduction and oxidation. This work studied a surface modification of Cu_2O with an n-type wide band gap semiconductor, that is SnO_2. The strategy consisted in creating a p-n junction that helps to draw photo-generated electrons from the Cu_2O into the n-type semiconductor to avoid the Cu_2O photo-corrosion. Indeed, tin oxide is an n-type direct band gap semiconductor with noticeable electron mobility (up to 250 $cm^2 V^{-1} s^{-1}$ [7]) as well as intrinsic stability. Besides, in general Sn-based materials are highly selective catalysts for the electrochemical (EC) CO_2RR to formate [8,9], which is currently reported as one highly desirable bulk chemicals in terms of economic and environmental benefits. Recent works highlight a strong dependence of Sn oxidation state versus the selectivity to a specific product [10,11]. Baruch et al. [12] observed by means of in-situ infrared spectroscopy that the CO_2RR proceeds over metallic Sn surface via a surface-bound carbonate (*OCHO) intermediate interacting with Sn(II) oxyhydroxide species. Instead, Zeng et al. [13] investigated the role of Sn(IV), in SnO_2 coupled with Cu_2O, as electrocatalyst for syngas production. Sn could become a barrier for further reduction of copper species, avoiding photo-electroactivity losses. According to literature, another effect of the Sn presence in the precursors solution is the diminishing of Cu_2O particles size [14,15], which can influence the adsorption/desorption of reaction intermediates and, consequently, the product distribution. Previous works

* Corresponding author.
E-mail address: simelys.hernandez@polito.it (S. Hernández).

https://doi.org/10.1016/j.cattod.2022.12.016
Received 31 August 2022; Received in revised form 27 October 2022; Accepted 21 December 2022
Available online 23 December 2022

have also documented the effectiveness of Cu-based material as (photo)-electrocatalysts for the EC CO_2RR in combination with Sn [16,17]. However, few studies have combined these materials in an easy synthesis route obtaining a stable photo-electrocatalyst for CO_2 reduction towards syngas and formate. Herein, the synthesis of a photoactive Cu-Sn-oxide-based catalyst for photo-electrocatalytic CO_2 reduction was optimised and standardised following an ultrasound-assisted co-precipitation method. The advantages of the sonochemical synthesis approach are significative: cost-effectiveness, high reaction rate, controllable synthesis condition, narrow size distribution, environmentally friendly nature and scalability [18,19]. This facile and scalable synthesis method allowed to obtain a stable photo-electrocatalyst with Cu^+ as main copper oxidation state, as confirmed by ex-situ characterizations before and after tests, which can be exploited as promising materials for the sun-driven CO_2 conversion.

2. Experimental section

2.1. Catalyst synthesis and characterization

In a typical synthesis, a Cu and Sn precursors solution (40 mL) was added to 200 mL of MilliQ water heated to 70 °C, in a completely

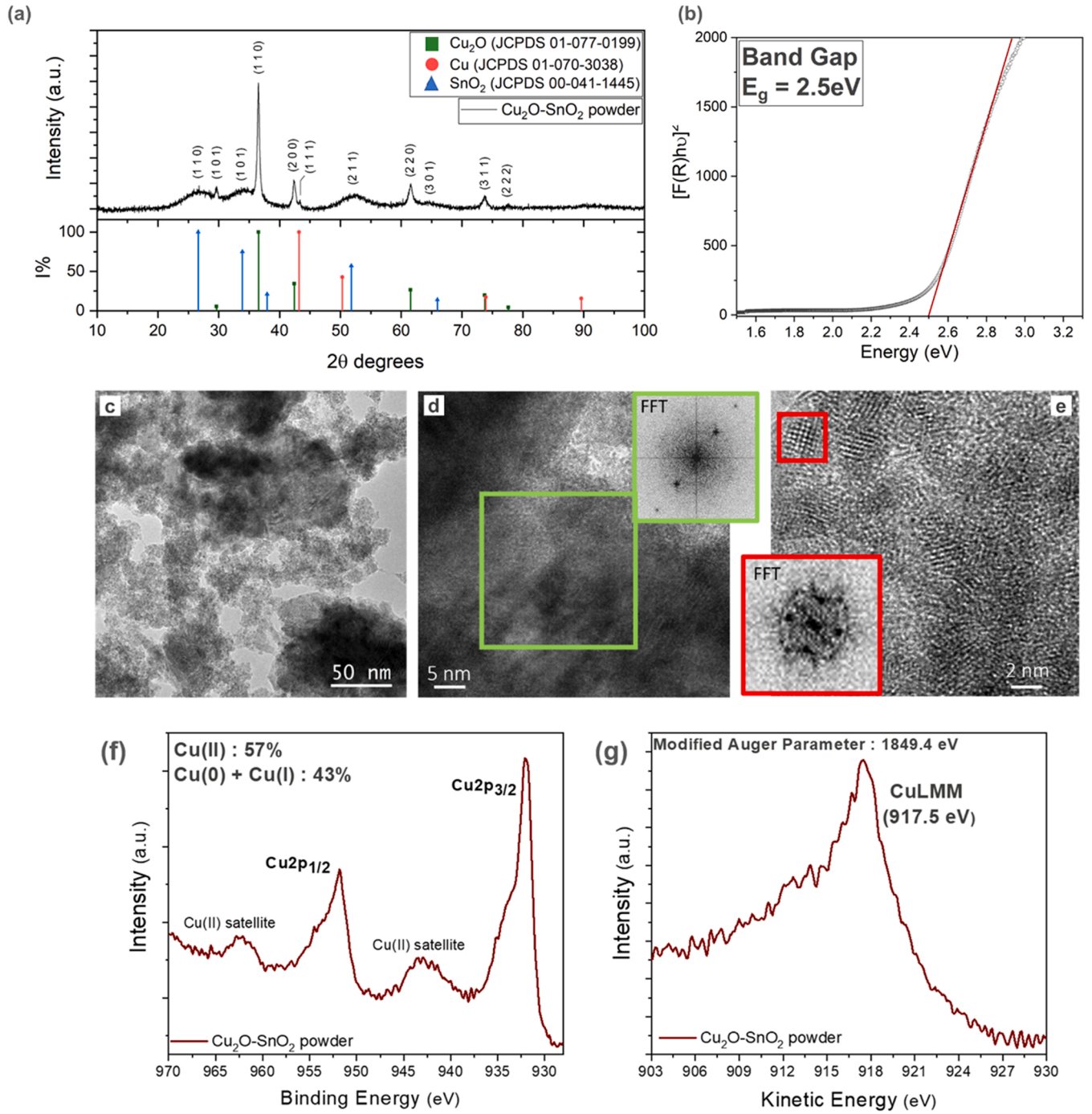

Fig. 1. (a) XRD pattern of the Cu_2O-SnO_2 powder catalyst; (b) Tauc's Plot for determining the material Band Gap; (c) Bright-Field TEM low magnification image and (d,e) High-Resolution TEM images with corresponding Fast Fourier Transform (FFT); XPS results of catalyst powder analysis: (f) high resolution $Cu2p_{1/2}$ and $Cu2p_{3/2}$ and abundance of copper oxidation states obtained from $Cu2p_{3/2}$ deconvolution procedure (not reported), (g) CuLMM spectra and Modified Auger Parameter value.

automatized way via a peristaltic pump (5 mL min^{-1} rate). The solution was maintained under agitation. A solution of Na_2CO_3 was used as the precipitant agent, which has been previously reported to result in slower growth kinetics than by using strong bases [20]. The addition occurs through a pump driven by a MC720 pH controller, sending the necessary amount of precipitating agent to maintain constant the pH at a value of 7. Finally, $NaBH_4$ was employed as reducing agent [21], aiming to promote the Cu_2O formation, and added by a peristaltic pump at a flow rate of 4 mL min^{-1}. The ultrasonic processor (Frequency: 20 kHz, amplitude of 30 %) was settled during the precipitation stage. The work-up, consisting of MilliQ water washings, was optimized to remove contaminants. After drying (60 °C), the catalyst was collected through in-vacuum filtration (with a nitrocellulose membrane filters, pore size 5 μm). Further details can be found in the Supporting Information (SI, Section S1). The reproducibility of the synthesis was assessed, details are in the SI, Section S2. The catalyst was characterized on its physico-chemical properties, as synthesised and in the electrode after its testing, by different techniques as detailed in the SI, Section S3.

2.2. Electrodes preparation and testing

The manufacturing process of the photo-electrodes was based on the preparation of a catalytic ink and its subsequent deposition on a porous carbon support (Toray carbon paper 060) by airbrushing [22]. The ink consisted of three components: the Cu_2O-SnO_2 catalyst, Nafion as the particles binder, and ethanol as a carrier for improving the dispersion. The mixture was sonicated for 30 min until an uniform slurry was obtained. Each electrode was prepared with a catalyst loading of 1 mg cm^{-2} in 1 cm^2 of active area, which was completely illuminated with simulated sunlight during the test. The photo-electrocatalytic tests for the CO_2RR were performed in an H-type electrochemical cell in aqueous media with the procedures specified in the SI, Section S4.

3. Results and discussion

3.1. Morphological and physical properties

The XRD pattern of the synthesised Cu_2O-SnO_2 sample is shown in Fig. 1a. A cubic crystalline phase (cuprite) of Cu_2O (JCPDS 01–077–0199) is evident with the most intense peak (111) at 2θ value of 36.5°. No peaks related to CuO were observed in the diffraction pattern. Metallic copper is also evident in a very small quantity, represented by the (111) peak at 43.3°, as a shoulder of the Cu_2O (200) peak at 42.3° (JCPDS 01–070–3039). Evidence of the SnO_2 presence (JCPDS 00–041–1445) was confirmed as well from its three most intense peaks at 2θ values of around 26.6° (110), 33.9° (200) and 51.8° (211), respectively. The presence of large bump distributed peaks, instead of a high intensity narrower shape, could lead to a double interpretation: tin oxide could be in the sample with its amorphous phase, as well as in so small sized crystallites that exhibits wide diffraction peaks because of their restricted number of reflection planes.

TEM characterization was performed to better understand the morphological and structural properties of the catalyst in the bulk and at the Cu–Sn-oxides interfaces. Bright field (BF) TEM images shown in Fig. 1c and Fig. S4a (SI, Section S5.1) evidence that various morphologies are present, namely large irregular particles and small particles, which is consistent with the FESEM observation. Large particles (100 nm) are decorated by smaller ones (1–10 nm). The large particles are not electronically transparent, therefore only limited signal can be detected from them both in TEM and in selected area electron diffraction (SAED) analysis. It was possible to determine the electron transparent regions that consist of edges of large particles and aggregates of nanoparticles, allowing for both the SAED analysis and high-resolution TEM imaging (HR-TEM). The electron diffraction pattern in Fig. S4b confirms the polycrystalline nature of the sample. Numerous reflections from various planes can be identified and ascribed to Cu_2O, CuO and SnO_2 (JCPDS 00–005–0667, JCPDS 00–048–1548, JCPDS 00–041–1445 cards, respectively). The 1st most internal ring represents SnO_2 and it is diffused, so SnO_2 is present in amorphous phase with some very small crystallites. Cu_2O is represented by the 2nd ring with only several spots, relative to the largest particles. These are mostly not electron transparent and therefore do not contribute to SAED. The 3rd and more external rings are assigned to CuO. It disagrees with what was observed by XRD analysis. However, different results can arise from these two techniques since they investigate a different portion of the material and with a different sensitivity. XRD penetrates all the material under investigation, while SAED signal can be acquired from electronically transparent parts of the sample; therefore, the large particles are not investigated. Only their edges and small particles contribute to the SAED pattern. The HRTEM investigation was performed on large particles by studying their edges or corners (TEM visible parts of these) and on smaller separate particles. Fig. 1d shows the HRTEM image of the edge of a large particle and the observed crystalline phase is confirmed by the Fast Fourier Transform (FFT shown in the inset) with interplanar spacing calculated from FFT of ~2.76 Å, which corresponds to (110) family of CuO structure planes. That agrees with SAED and suggest that a few amount of Cu^{+1} was oxidized to Cu^{+2}. Fig. 1e shows HR-TEM image and corresponding FFT pattern of small crystallites, which can be found everywhere in the sample, and cover the large copper-based particles. This analysis confirms the presence of amorphous material and very small SnO_2 crystallites. It is in accordance with XRD, where a very broad peak for SnO_2 was observed, and SAED, where a high diffuse ring was observed. Moreover, the optical band gap (E_g) of the samples was calculated by using the Tauc's method [23] from the F(R) spectra, obtained by using a spectrophotometer in the diffuse reflectance mode with an integrating sphere. The resulting plot can be observed in Fig. 1b. The obtained band gap value of 2.5 eV agrees with results found in literature on similar structures [24]. The increase in energy of the synthesised catalyst with respect to bare Cu_2O could be useful to avoid photo-corrosion issues in aqueous solution during PEC CO_2 reduction tests, due to the redox reaction of Cu_2O itself [25,26]. Therefore, successfully ensuring a protective layer on the surface of Cu_2O could be the key factor for a long-timing life catalyst. Herein, the surface presence of SnO_2 has increased the E_g value of the photo-electrocatalyst thanks to its higher band gap values (3.58–3.45 eV) [27]. The investigation on copper oxidation states at the catalyst surface was carried out by XPS analysis. The High-Resolution analysis of Cu species is shown in Fig. 1f, and the doublet shape has been compared with values reported in the literature [28]. The presence of the well-known shake-up satellite found in Cu2p spectra is an indication of the presence of Cu^{+2} species. A deconvolution procedure [29], performed on $Cu2p_{3/2}$ peak and the related shake-up satellite to evaluate the relative abundance of Cu^{+2} and $Cu^0 + Cu^{+1}$ oxidation states, led to the following results: 57 % of Cu^{+2} and 43 % of $Cu^0 + Cu^{+1}$. In addition to the Auger parameter, the CuLMM peak shape (Fig. 1g) can also be useful in revealing the copper chemical states. It is particularly important when determining metallic Cu versus Cu^{+1}. By using Eq. 1:

$$Auger\ \ parameter = hv - CuLMM + Cu2p_{3/2} \quad (1)$$

a value of 1849.4 eV was obtained. It was compared with the value of 1849.17 ± 0.03 eV referred to Cu_2O [30], thus enabling the average oxidation state of superficial copper in the whole sample to be assessed as Cu^{+1}. Regarding the Sn oxide, the typical shape of XPS valence band spectra of SnO_2 (Fig. S5a) with a maximum at ~2.5 eV is distinctive of Sn^{+4} and allow to distinguish it from Sn^{+2}, which has a similar binding energy position related to Sn3d doublet (Fig. S5b). Based on the previous information, it can be affirmed that the desired Cu_2O-SnO_2 structure was obtained with the presence of some Cu^{+2} at the material surface, which could be due to the partial oxidation of the Cu^{+1} after the synthesis process. Finally, by means of XPS high resolution analysis in the valence band region, the valence band maximum (VBM) position was

extrapolated (Fig. S5a), with a linear fit applied to the descending portion of the signal towards the 0 eV point, corresponding to the Fermi level. Due to the noisy signal of this region (which possesses a low emission cross section with X-ray source), the result obtained is affected by a huge standard deviation (-0.16 ± 0.40) eV. Thus, even if it is not possible to rely on this exact value, it can be stated that a change in the Cu_2O band structure was introduced, thanks to the outer SnO_2 modification, since a localised band bending was created, due to new available populated energy levels. The result of the p-n junction due to Cu_2O and SnO_2 interface shows a new region which possesses an excess of electrons nearby the Fermi Energy Level of the catalyst. Other information about the characterization of the as synthesised catalyst, as well as of the electrodes (before and after testing) are reported in the SI, Sections S5.1 and S5.2 and discussed therein and in following.

3.2. Photo-electrocatalytic (PEC) CO_2 reduction test

Firstly, blank tests were performed and demonstrate the absence of photoactivity for the CO_2RR of the carbon-based substrate (see SI, Section S6). Then, the PEC behaviour of Cu_2O-SnO_2 electrode was evaluated for the photo-electroreduction of CO_2 in an aqueous 0.1 M $KHCO_3$ solution, using as illumination source a solar simulator. The cyclic voltammetry (CV) curves obtained by saturating the celectrolyte with N_2 or CO_2 are shown in Fig. 2a. The onset potential is the lowest potential value at which a reaction product is formed (a Faradaic current is measured) with a given electrode under defined conditions. Herein, the

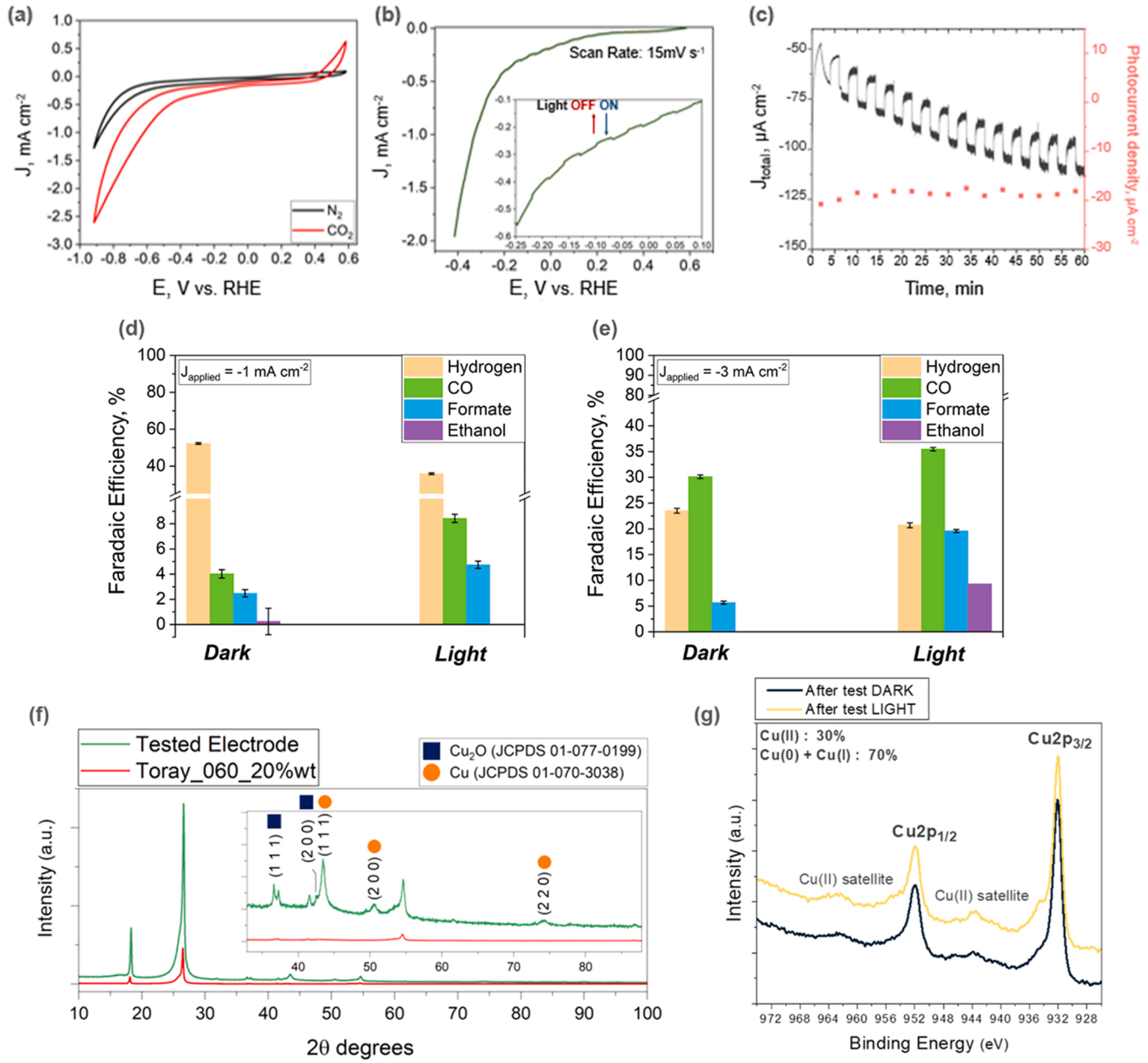

Fig. 2. PEC test of CO_2 reduction; (a) Cyclic Voltammetry performed in N_2 and CO_2; (b) Linear Sweep Voltammetry performed in CO_2-environment with chopped light; (c) Chronoamperometry test performed at − 250 mV, pointing out the stability of the photocurrent density (red dots). FEs of gas and liquid products detected after a 2-hours Chronopotentiometry in 0.1 M $KHCO_3$ aqueous electrolyte at (d) − 1 mA cm^{-2} and (e) − 3 mA cm^{-2}. For each current density value, the products are reported both for the test without and under illumination. (f) XRD pattern of Carbon Paper (electrodes support) (red line) and the electrode with the Cu_2O-SnO_2 catalyst after the test under light conditions (green line). In the inset the peaks attributed to catalyst are reported and labelled; (g) XPS High-Resolution spectra of two electrodes one after a test in dark (blue line) the other after a test in light (yellow line), focusing on the copper peaks.

onset potential diminished by changing from the inert environment to the CO_2 saturated solution. In fact, there is a difference of around 0.2 V vs. RHE passing from N_2 (−0.67 V vs. RHE) to CO_2 (−0.46 V vs. RHE). The reduced CO_2RR onset potential indicates a higher catalytic activity in CO_2 than in N_2 and the first H^+/e^- transfer to form a C-based intermediate specie at the electrode surface [31]. Fig. 2b shows the linear sweep voltammetry (LSV) pattern recorded with a scan rate of 15 mV s^{-1} under chopped illumination (Δt=2 s). The inset demonstrates the behaviour of the cathodic current under the effect of light at low potential values: it increases when light is on (blue arrow), conversely, it diminishes in dark conditions (red arrow). A sudden increase in the absolute photocurrent value was observed during the enlightenment since a part of the energy required for the CO_2 reduction is currently provided by the internal photovoltage generated by the photocatalyst material under simulated sunlight illumination. This increment reached a maximum (0.02 mA) at about 0.1 V vs RHE. The onset potential was identified at − 0.1 V vs. RHE at a current density value of about − 0.3 mA cm^{-1}, and the photocurrent started decreasing at − 0.2 V vs RHE, because the onset of the dark Faradaic current exceeds the photoactivity gain. Chronoamperometry tests were done under the alternance of dark and light conditions by applying a fixed potential of −250 mV to show the catalyst photoactivity. As reported in Fig. 2c, the photocurrent density was maintained stable for 1 h (red dots), evidencing the whole system stability, even when the total current density increases in absolute value (grey line). The net photocurrent density value stands to −18 μA cm^{-2}. As reported in previous works [32], the presence of SnO_2 coupled to Cu_2O showed improved performances with respect to the bare Cu_2O (see SI, Section S7.1), as another proof of the protection role proposed for tin oxide towards Cu_2O stability. Further insights of PEC tests and an analysis of the evolution of the gaseous products over time can be found in the SI (Section S7.2). Fig. 2d and Fig. 2e exhibit the Faradaic efficiencies (FEs) achieved for the test carried out in dark and light conditions. The values were obtained by applying Equation S3 (in SI) after a chronopotentiometry test of 2 h at two different current densities of − 1 mA cm^{-2} and − 3 mA cm^{-2}. In both cases, the CO_2 reduction products (mainly CO and formate) increased in lighting conditions. In fact, at − 1 mA cm^{-2}, the FE toward H_2 decreased by 30 % under illumination with respect to the dark test, while the total FE of C-based products doubled, reaching around 13 %. A similar behaviour was also identified in the two tests at − 3 mA cm^{-2}: the reduction of the FE_{H2} was observed under light conditions, but this time in a more limited way (passing from 23.5 % to 20.7 %). Respect to the previous case, a smaller increase (~ 18 %) in the CO production was noticed under illumination at − 3 mA cm^{-2}, reaching a FE_{CO} of 35.5 %. The main differences are related to the other C-based products. Indeed, the FE towards formate increased by about four times (5.7 % in dark vs. 19.6 % in light) and ethanol, which was no detected among the liquid products during the dark test, was produced with a FE of 9.3 % under light irradiation. The rising value of FE_{CO} at expenses of the FE_{H2} was also reported by Zeng et al. [13] during the electrocatalytic CO_2RR with a Cu-Sn based foam. Moving from − 0.5 to − 0.6 V vs. RHE, they observed a FE_{CO} gain to ~15 % while the FE_{H2} was more than halved. A similar trend was found by Zhang et al., [33] by using Cu_2O-nanowires as bare catalyst and decorated with SnO_x particles, for syngas production. Herein, this phenomenon is present for both bare Cu_2O (see SI, Section S7.1) and Cu_2O-SnO_2-based electrodes. In fact, more negative potentials led to a higher amount of CO with respect to H_2, higher cathodic current densities and higher negative potentials (driving force) onto the electrode, at which the CO_2 reduction is favoured over the H_2 evolution reaction. Finally, by comparing previous electrocatalytic versus PEC CO_2RR results, Zhang et al. [33] data showed higher FE for CO under illumination tahn under dark conditions with Cu_2O nanowires, at different applied potentials, confirming that the CO_2RR is strongly favoured due to the illumination, like in our experiments. On the other hand, they observed a CO/H_2 ratio higher than ours: they reached the maximum of ~4.5 by applying − 0.35 V vs. RHE while herein a CO/H_2 ratio of 1.7 was obtained in the test at − 3 mA cm^{-2}. This could be due to the different catalyst properties or experimental set-ups but also indicates the necessity to further investigate the role of different applied potentials and current density values. Nonetheless, with the here reported synthetic approach, the developed Cu_2O-SnO_2 catalyst was also selective for ethanol production at − 3 mA cm^{-2}, which requires the more difficult C-C coupling, and more than doubled the FE to formate if compared to Zhang and co-worker's results. Therefore, we believed that the prepared Cu_2O-SnO_2 catalyst could be used not only in the PEC CO_2RR processes to produce syngas but also formate and other high value-added molecules. It is worth to mention that Chen and co-workers [34] studied the dependence of the current densities for producing some CO_2 reduction products (CO, Formate) as a function of the illumination intensity. They obtained that the current density for all the products increased as the illumination intensity increased and the products distribution varied as a function of the applied potential. That behaviour is because the simulated sunlight provide an extra energy source that generate separated photocarriers and excite electrons that are then able to participate in the CO_2R reaction with a lower external energy consumption, leading to easier production of C_{1+} compounds [35]. In addition, the use of visible light seems to be highly appealing for the photo-excitation of the CO_2 radical anion, known as the first activated intermediate specie of CO_2, before its reduction in a multi-step mechanism to produce either formate, CO or C_2^+ products [36]. Indeed, C_2 products are favoured in the presence of Cu^{+1} and Cu^0 interfaces at the catalyst surface that could promote dimerization of *CO or *CH_x adsorbed intermediates [37]. On the other hand, the reason behind the not null dark currents is because CO_2 is converted even in dark conditions on Cu-based catalysts, whose performance is among the best that has ever been achieved for CO_2 electroreduction to > C_{1+} and multicarbon products [38,39]. Thus, herein, the CO_2 reduction is noticeably enhanced under light irradiation thanks to the photovoltage generated at the irradiated semiconductor/solution junction, and to the photo-generated electrons with the energy required for the CO_2 reduction to C_{1+} products. Moreover, the SnO_2 presence on Cu_2O particles could lead to an internal electric field thanks to which the photogenerated carries could be separated and the photoelectrons can take part on the reduction reaction. Indeed, the stability reached in the 1-hour long test could be seen a proof of the inhibition of photo-corrosion of Cu_2O due to the improved transfer of photogenerated carriers.

3.3. After PEC test electrodes characterization

Ex-situ XRD and XPS characterisations were performed on the tested electrodes to investigate the eventual modification of the copper oxidation state that occurred under the PEC CO_2R conditions. Both analyses demonstrated that the crystalline phase composition partially changed during the test. XRD analysis, shown in Fig. 2 f, is dominated by the contribution from the support, therefore, we focus on the part of the spectrum in the inset. The XRD characterization indicates that only two peaks attributed to Cu_2O remained visible in the diffractogram (36.5° and 42.4°) collected from the tested electrode. The remaining diffraction peaks refer to metallic copper (JCPDS 01–070–3039), such as (200), (220) and (311) placed at 50.3°, 73.9° and 89.9°, respectively. Moreover, XPS analysis on the tested electrodes in dark and light conditions are shown in Fig. 2g. As a further confirmation of the change in oxidation state, XPS analysis of tested electrodes revealed a remarkable reduction of the Cu^{+2} and an increase in the Cu^{+1} +Cu^0 percentage, with respect to results on the not tested electrodes (SI, Section S5.2). The presence of about 30 % of Cu^{+2} and 70 % of Cu^{+1} + Cu^0 from the Cu2p HR spectra was assessed on both dark and light tested electrodes. Indeed, in most cases, the overall FE value is less than 100 % and the partial reduction of the copper species could have a role in this fact. As it is well-know, previous Cu_2O-based photo-electrocatalysts for CO_2RR still suffer from poor stability due to the reduction of Cu^{1+} to Cu^0.

Further efforts are needed to enhance and maintain their current densities to significant values without losses in catalytic structure or changing of morphology and oxidation states. However, Auger's parameters calculation (Eq. 1) applied to CuLMM spectra of our tested samples (values of 1849.2 eV and 1849.1 for the electrode tested in dark and in light conditions, respectively) confirmed that Cu^{+1} is the average copper oxidation state at the catalyst surface. Hence, although in the catalyst bulk the Cu_2O was reduced to Cu^0 (as shown from the XRD data), the XPS results demonstrate how valuable the here reported synthesis method is to incorporate SnO_2 having a role as protector of the Cu^{+1} superficial states.

4. Conclusions

In this work, a facile, scalable, and reproducible method for the synthesis of Cu_2O-SnO_2 catalyst was developed. Several analytical techniques were used to characterize the samples and assess the synthesis reproducibility. Cu^{+1} was found as the average and more abundant copper oxidation state and no remarkable traces of contaminants were observed either in the bulk and surface of the catalyst. With the aim to understand how the light could affect the products formation, PEC CO_2 reduction tests both in dark and light conditions were performed. An enhancement towards C-based compounds was achieved in the tests under illumination. To the best of our knowledge, this is among the first studies that has investigated the trend of gaseous and liquid C-based products with Cu_2O-SnO_2 nanoparticle-based catalysts, demonstrating the role of light in promoting not only C_1 (CO and formate) but also C_2 products like ethanol at low potential values. This is a key and useful result to tune the catalyst selectivity towards the desired CO_2 products. A high attention was also paid to the catalyst restructuration, focusing on the changes in the copper oxidation state. Cu^{+1} was assessed as the average oxidation state in the surface of tested electrodes, which confirms the effectiveness of the here proposed synthesis approach for stabilising Cu_2O (the only photoactive Cu species) by SnO_2 nanoparticles, while in the bulk it was evident a partial reduction of Cu^{+1} to Cu^0. Tuning the synthesis process parameters to modify the particles size could be a future strategy to enhance the amount of active superficial sites and limit the bulk Cu formation. Moreover, the long-term stability at high current densities remains a challenging aspect to face. However, due to their high abundance and unique photo-catalytic properties of Cu_2O-based materials, the here developed catalyst can offer a promising platform to utilize solar energy and convert CO_2 into useful products.

CRediT authorship contribution statement

Maddalena Zoli: Catalysts synthesis, Photo-electrochemical Investigation, Data curation, Formal analysis, Writing – original draft, **Daniela Roldán:** Catalysts synthesis, Validation, **Hilmar Guzmán:** Conceptualization, Catalysts synthesis and Validation, Methodology, Photo-electrochemical, Formal analysis, Writing – review & editing. **Micaela Castellino:** XPS Investigation, Formal analysis, Writing – review & editing, **Angelica Chiodoni:** TEM and XRD Investigation, Formal analysis, Writing – review & editing, **Katarzyna Bejtka:** TEM and XRD Investigation, Formal analysis, Writing – review & editing, **Nunzio Russo:** Resources, Supervision, Writing – review & editing, **Simelys Hernández:** Conceptualization, Methodology, Photo-electrochemical, Formal analysis, Funding acquisition, Resources, Supervision, Writing – review & editing, All authors have read and agreed to the published version of the manuscript.

Declaration of Competing Interest

The authors declare the following financial interests/personal relationships which may be considered as potential competing interests: Simelys Hernandez reports financial support was provided by European Union.

Data Availability

Data will be made available on request.

Acknowledgments

This work has received funding from the European Union's Horizon 2020 Research and Innovation Action programme under the Project SunCoChem (Grant Agreement No 862192).

Appendix A. Supporting information

Supplementary data associated with this article can be found in the online version at doi:10.1016/j.cattod.2022.12.016.

References

[1] H. Guzmán, N. Russo, S. Hernández, CO_2 valorization towards alcohols by Cu-based electrocatalysts: challenges and perspectives, Green. Chem. 23 (2021) 1896–1920, https://doi.org/10.1039/d0gc03334k.
[2] H. Guzmán, F. Salomone, E. Batuecas, T. Tommasi, N. Russo, S. Bensaid, S. Hernández, How to make sustainable CO_2 conversion to methanol: thermocatalytic versus electrocatalytic technology, Chem. Eng. J. 417 (2021), https://doi.org/10.1016/j.cej.2020.127973.
[3] A.D. Handoko, J. Tang, Controllable proton and CO2 photoreduction over Cu2O with various morphologies, in: Int. J. Hydrogen Energy, 2013: pp. 13017–13022. ⟨https://doi.org/10.1016/j.ijhydene.2013.03.128⟩.
[4] J.C. Wang, L. Zhang, W.X. Fang, J. Ren, Y.Y. Li, H.C. Yao, J.S. Wang, Z.J. Li, Enhanced photoreduction CO_2 activity over direct Z-Scheme α-Fe2O3/Cu2O heterostructures under visible light irradiation, ACS Appl. Mater. Interfaces 7 (2015) 8631–8639, https://doi.org/10.1021/acsami.5b00822.
[5] H. Guzmán, M.A. Farkhondehfal, K.R. Tolod, S. Hernández, N. Russo, Photo/electrocatalytic hydrogen exploitation for CO_2 reduction toward solar fuels production, in: Sol. Hydrog. Prod., Elsevier, 2019, pp. 365–418, https://doi.org/10.1016/B978-0-12-814853-2.00011-4.
[6] A. Paracchino, V. Laporte, K. Sivula, M. Grätzel, E. Thimsen, Highly active oxide photocathode for photoelectrochemical water reduction, Nat. Mater. 10 (2011) 456–461, https://doi.org/10.1038/nmat3017.
[7] H. Mun, H. Yang, J. Park, C. Ju, K. Char, High electron mobility in epitaxial SnO2-x in semiconducting regime, APL Mater. 3 (2015), https://doi.org/10.1063/1.4927470.
[8] M. Li, X. Tian, S. Garg, T.E. Rufford, P. Zhao, Y. Wu, A.J. Yago, L. Ge, V. Rudolph, G. Wang, Modulated Sn oxidation states over a Cu2O-derived substrate for selective electrochemical CO_2 reduction, ACS Appl. Mater. Interfaces 12 (2020) 22760–22770, https://doi.org/10.1021/acsami.0c00412.
[9] S. Zhao, S. Li, T. Guo, S. Zhang, J. Wang, Y. Wu, Y. Chen, Advances in Sn-based catalysts for electrochemical CO_2 reduction, Nano-Micro Lett. 11 (2019), https://doi.org/10.1007/s40820-019-0293-x.
[10] A. Dutta, A. Kuzume, M. Rahaman, S. Vesztergom, P. Broekmann, Monitoring the chemical state of catalysts for CO_2 electroreduction: an in operando study, ACS Catal. 5 (2015) 7498–7502, https://doi.org/10.1021/acscatal.5b02322.
[11] Y. Chen, M.W. Kanan, Tin oxide dependence of the CO 2 reduction efficiency on tin electrodes and enhanced activity for tin/tin oxide thin-film catalysts, J. Am. Chem. Soc. 134 (2012) 1986–1989, https://doi.org/10.1021/ja2108799.
[12] M.F. Baruch, J.E. Pander, J.L. White, A.B. Bocarsly, Mechanistic insights into the reduction of CO_2 on tin electrodes using in situ ATR-IR spectroscopy, ACS Catal. 5 (2015) 3148–3156, https://doi.org/10.1021/acscatal.5b00402.
[13] J. Zeng, K. Bejtka, W. Ju, M. Castellino, A. Chiodoni, A. Sacco, M.A. Farkhondehfal, S. Hernández, D. Rentsch, C. Battaglia, C.F. Pirri, Advanced Cu-Sn foam for selectively converting CO_2 to CO in aqueous solution, Appl. Catal. B Environ. 236 (2018) 475–482, https://doi.org/10.1016/j.apcatb.2018.05.056.
[14] R. Chen, Z. Wang, Q. Zhou, J. Lu, M. Zheng, A template-free microwave synthesis of one-dimensional Cu2O nanowires with desired photocatalytic property, Materials 11 (2018) 1843, https://doi.org/10.3390/ma11101843.
[15] Y. Du, N. Zhang, C. Wang, Photo-catalytic degradation of trifluralin by SnO2-doped Cu2O crystals, Catal. Commun. 11 (2010) 670–674, https://doi.org/10.1016/j.catcom.2010.01.021.
[16] Y. Zhao, C. Wang, G.G. Wallace, Tin nanoparticles decorated copper oxide nanowires for selective electrochemical reduction of aqueous CO_2 to CO, J. Mater. Chem. A 4 (2016) 10710–10718, https://doi.org/10.1039/c6ta04155h.
[17] X. Jiang, X. Wang, Z. Liu, Q. Wang, X. Xiao, H. Pan, M. Li, J. Wang, Y. Shao, Z. Peng, Y. Shen, M. Wang, A highly selective tin-copper bimetallic electrocatalyst for the electrochemical reduction of aqueous CO_2 to formate, Appl. Catal. B Environ. 259 (2019), 118040, https://doi.org/10.1016/j.apcatb.2019.118040.
[18] R. Sakthivel, S. Kubendhiran, S.-M. Chen, Facile one-pot sonochemical synthesis of Ni doped bismuth sulphide for the electrochemical determination of promethazine hydrochloride, Ultrason. Sonochem. 54 (2019) 68–78, https://doi.org/10.1016/j.ultsonch.2019.02.013.
[19] R. Singh Yadav, I. Kuřitka, J. Vilcakova, T. Jamatia, M. Machovsky, D. Skoda, P. Urbánek, M. Masař, M. Urbánek, L. Kalina, J. Havlica, Impact of sonochemical synthesis condition on the structural and physical properties of MnFe2O4 spinel

ferrite nanoparticles, Ultrason. Sonochem. 61 (2020), 104839, https://doi.org/10.1016/j.ultsonch.2019.104839.
[20] C. Blanco-Andujar, D. Ortega, Q.A. Pankhurst, N.T.K. Thanh, Elucidating the morphological and structural evolution of iron oxide nanoparticles formed by sodium carbonate in aqueous medium, J. Mater. Chem. 22 (2012) 12498, https://doi.org/10.1039/c2jm31295f.
[21] L. Lu, X. Sun, J. Ma, D. Yang, H. Wu, B. Zhang, J. Zhang, B. Han, Highly efficient electroreduction of CO_2 to methanol on palladium–copper bimetallic aerogels, Angew. Chem. - Int. Ed. 57 (2018) 14149–14153, https://doi.org/10.1002/anie.201808964.
[22] H. Guzmán, F. Zammillo, D. Roldán, C. Galletti, N. Russo, S. Hernández, Investigation of gas diffusion electrode systems for the electrochemical CO_2 conversion, Catalysts 11 (2021), https://doi.org/10.3390/catal11040482.
[23] K. Madhusudan Reddy, S.V. Manorama, A. Ramachandra Reddy, Bandgap studies on anatase titanium dioxide nanoparticles, Mater. Chem. Phys. 78 (2003) 239–245, https://doi.org/10.1016/S0254-0584(02)00343-7.
[24] L. Liu, W. Sun, W. Yang, Q. Li, J.K. Shang, Post-illumination activity of SnO2 nanoparticle-decorated Cu2O nanocubes by H2O2 production in dark from photocatalytic "memory", Sci. Rep. 6 (2016) 20878, https://doi.org/10.1038/srep20878.
[25] M. Schreier, J. Luo, P. Gao, T. Moehl, M.T. Mayer, M. Grätzel, Covalent immobilization of a molecular catalyst on Cu $_2$ O photocathodes for CO $_2$ reduction, J. Am. Chem. Soc. 138 (2016) 1938–1946, https://doi.org/10.1021/jacs.5b12157.
[26] D.H. Won, C.H. Choi, J. Chung, S.I. Woo, Photoelectrochemical production of formic acid and methanol from carbon dioxide on metal-decorated CuO/Cu2O-layered thin films under visible light irradiation, Appl. Catal. B Environ. 158–159 (2014) 217–223, https://doi.org/10.1016/j.apcatb.2014.04.021.
[27] N. Kamarulzaman, N.D. Abdul Aziz, M.F. Kasim, N.F. Chayed, R.H. Yahaya Subban, N. Badar, Anomalies in wide band gap SnO2 nanostructures, J. Solid State Chem. 277 (2019) 271–280, https://doi.org/10.1016/j.jssc.2019.05.035.
[28] M.C. Biesinger, L.W.M. Lau, A.R. Gerson, R.S.C. Smart, Resolving surface chemical states in XPS analysis of first row transition metals, oxides and hydroxides: Sc, Ti, V, Cu and Zn, Appl. Surf. Sci. 257 (2010) 887–898, https://doi.org/10.1016/j.apsusc.2010.07.086.
[29] M.C. Biesinger, B.R. Hart, R. Polack, B.A. Kobe, R.S.C. Smart, Analysis of mineral surface chemistry in flotation separation using imaging XPS, Miner. Eng. 20 (2007) 152–162, https://doi.org/10.1016/j.mineng.2006.08.006.
[30] D. Briggs, Handbook of X-ray Photoelectron Spectroscopy C. D. Wanger, W. M. Riggs, L. E. Davis, J. F. Moulder and G. E.Muilenberg Perkin-Elmer Corp., Physical Electronics Division, Eden Prairie, Minnesota, USA, 1979. 190 pp. $195, Surf. Interface Anal. 3 (1981) v–v. ⟨https://doi.org/10.1002/sia.740030412⟩.
[31] J.T. Billy, A.C. Co, Reducing the onset potential of CO_2 electroreduction on CuRu bimetallic particles[1] J.T. Billy, A.C. Co, Reducing the onset potential of CO_2 electroreduction on CuRu bimetallic particles, Appl. Catal. B Environ. 237 (2018) 911–918, https://doi.org/10.101, Appl. Catal. B Environ. 237 (2018) 911–918. https://doi.org/10.1016/J.APCATB.2018.06.072.
[32] J. Yuan, B. Xiao, C. Hao, Photoelectrochemical reduction of carbon dioxide to ethanol at Cu2O foam cathode, Int. J. Electrochem. Sci. 12 (2017) 8288–8294, https://doi.org/10.20964/2017.09.36.
[33] Y. Zhang, D. Pan, Y. Tao, H. Shang, D. Zhang, G. Li, H. Li, Photoelectrocatalytic reduction of CO_2 to syngas via SnOx-enhanced Cu2O Nanowires Photocathodes, Adv. Funct. Mater. 32 (2022), https://doi.org/10.1002/adfm.202109600.
[34] Y. Chen, N.S. Lewis, C. Xiang, Modeling and simulation of the spatial and light-intensity dependence of product distributions in an integrated photoelectrochemical CO_2 reduction system, ACS Energy Lett. 1 (2016) 273–280, https://doi.org/10.1021/acsenergylett.6b00134.
[35] P. Chen, Y. Zhang, Y. Zhou, F. Dong, Photoelectrocatalytic carbon dioxide reduction: fundamental, advances and challenges, Nano Mater. Sci. 3 (2021) 344–367, https://doi.org/10.1016/J.NANOMS.2021.05.003.
[36] C.M. Hendy, G.C. Smith, Z. Xu, T. Lian, N.T. Jui, Radical chain reduction via carbon dioxide radical anion (CO_2•-), J. Am. Chem. Soc. 143 (2021) 8987–8992, https://doi.org/10.1021/jacs.1c04427.
[37] H. Guzmán, F. Salomone, S. Bensaid, M. Castellino, N. Russo, S. Hernández, CO2Conversion to alcohols over Cu/ZnO catalysts: prospective synergies between electrocatalytic and thermocatalytic routes, ACS Appl. Mater. Interfaces 14 (2022) 517–530, https://doi.org/10.1021/acsami.1c15871.
[38] J.F. de Brito, A.R. Araujo, K. Rajeshwar, M.V.B. Zanoni, Photoelectrochemical reduction of CO_2 on Cu/Cu2O films: product distribution and pH effects, Chem. Eng. J. 264 (2015) 302–309, https://doi.org/10.1016/j.cej.2014.11.081.
[39] R. Kortlever, K.H. Tan, Y. Kwon, M.T.M. Koper, Electrochemical carbon dioxide and bicarbonate reduction on copper in weakly alkaline media, J. Solid State Electrochem. 17 (2013) 1843–1849, https://doi.org/10.1007/s10008-013-2100-9.